aerospace

MDPI

*Article*

# An Optimization Study of Circumferential Groove Casing Treatment in a High-Speed Axial Flow Compressor

**Wenhao Liu, Wuli Chu *, Haoguang Zhang and Hao Wang**

School of Power and Energy, Northwestern Polytechnical University, Xi'an 710129, China; whliu@mail.nwpu.edu.cn (W.L.); zhg@nwpu.edu.cn (H.Z.); hao1999@mail.nwpu.edu.cn (H.W.)
* Correspondence: wlchu@nwpu.edu.cn

**Abstract:** In this paper, a numerical optimization study of single-groove casing treatment was conducted on a high-speed axial compressor. One of the aims is to find the optimal structure of a single groove that can improve compressor stability with minimal loss in efficiency. Another aim is to explore suitable parameters for rapidly evaluating the compressor stall margin. A design optimization platform has been constructed in this paper, which utilizes NSGA-II and a Radial Basis Function (RBF) neural net model to carry out the optimization. The stall margin of the compressor with A single groove was accurately determined by calculating its entire overall performance line. A Pareto front is obtained through optimization, and the optimal design can be selected from the Pareto front. By considering both stall margin and efficiency loss, one of the optimal designs was found to achieve a 7.49% improvement in stall margin with a 0.24% improvement in peak efficiency. Based on the database, the effect of design parameters of a single groove on compressor stability and performance is analyzed. A series of evaluation parameters of stall margin were compared to their degree of correlation with the real stall margin calculated by the entire overall performance line. As a result, tip blockage and momentum ratio can be used as efficient parameters for quickly evaluating the compressor stall margin without the need to calculate the entire performance curve of the compressor.

**Keywords:** axial flow compressor; stability; performance; groove; optimization design

check for updates

**Citation:** Liu, W.; Chu, W.; Zhang, H.; Wang, H. An Optimization Study of Circumferential Groove Casing Treatment in a High-Speed Axial Flow Compressor. *Aerospace* **2024**, *11*, 541. https://doi.org/10.3390/aerospace11070541

Academic Editor: Kung-Ming Chung

Received: 15 April 2024
Revised: 30 May 2024
Accepted: 18 June 2024
Published: 1 July 2024

**Copyright:** © 2024 by the authors. Licensee MDPI, Basel, Switzerland. This article is an open access article distributed under the terms and conditions of the Creative Commons Attribution (CC BY) license (https://creativecommons.org/licenses/by/4.0/).

## 1. Introduction

Compressor aerodynamic stability has been one of the research hotspots in the field of turbomachinery. Aerodynamic instability usually manifests itself as stall and surge. Compressor aerodynamic instability can seriously affect the stable operation of the compressor and the entire engine [1–3]. Therefore, it is very important to find methods to postpone the occurrence of compressor aerodynamic instability and extend the stable operating range of the compressor. After years of research and development, two types of flow control methods have been formed: passive control and active control. Among them, the casing treatment, as a passive control method, has been widely studied by researchers. The casing treatment was first accidentally discovered in an experiment conducted by NASA [4]. Since then, the casing treatment has been widely studied. Among them, for the "groove-type" casing treatment, the grooves are arranged in the circumferential direction of the rotor, which is usually called circumferential grooves. It can obtain a relatively small improvement in stability margin but can slightly reduce or basically not reduce the compressor efficiency [5,6].

A large amount of research has been conducted on groove casing treatment. Most of the research has focused on the stability enhancement mechanism of casing treatment and its geometric parameter design. The stability enhancement mechanism of groove casing treatment has been well understood, and a wealth of design experience has been accumulated. However, the selection of geometric design parameters of groove casing treatment

is mainly based on experience. It is difficult to design groove casing treatment that can simultaneously take into account the stability margin and efficiency of the compressor. In recent years, research on geometric optimization of casing treatment using optimization algorithms has gradually become a hot topic. This provides a solution to obtain a casing treatment structure that can simultaneously take into account the stability margin and efficiency of the compressor. The studies of multi-objective optimization design of casing treatment are relatively rare. Vuong et al. [7] conducted multi-objective optimization research on the combined self-recirculating and circumferential groove casing treatment for the NASA Stage 37 transonic axial compressor stage and obtained the casing treatment structure with the maximum stability margin and minimum efficiency loss. Goinis et al. [8] used unsteady numerical simulation methods to conduct multi-objective optimization design research of axial slot casing treatment on a transonic compressor, with efficiency and stability margin improvement as the objective function. They obtained the Pareto-optimal axial slot casing treatment. The study results pointed out that the slot-type casing that can effectively improve the stability margin of the compressor should have the following characteristics: the axial position is close to the tip leading edge, the angle of the slot is opposite to the installation angle of the blade, and the slot is inclined in the radial direction. The open area and shape of the slot determine the effectiveness of the stabilizing effect. Goinis et al. [9] also conducted similar optimization studies on circumferential groove casing treatment. Kim et al. [10] used a hybrid multi-objective evolutionary algorithm and surrogate model to conduct multi-objective optimization research on the combined circumferential slot casing and tip injection. Stability margin and peak efficiency were selected as objective functions. According to the Pareto optimal solution, the two objective functions were traded off. The optimized casing treatment successfully improved the stability margin and peak efficiency of the compressor compared to the solid casing. Zhao et al. [11] conducted multi-objective optimization design research for circumferential groove casing treatment on the NASA Rotor 37. The objective functions were stability margin and peak efficiency. The optimization variables were the tip gap and groove width. Latin hypercube sampling was used to sample, and the NSGA-II multi-objective evolutionary algorithm was used to find the Pareto optimal solution. Finally, two results were selected, and relevant numerical studies were conducted to discuss the stabilizing mechanism of circumferential grooves. Zhu [12] used the NSGA-II multi-objective optimization algorithm to optimize the coupling of the single circumferential groove and the first-stage rotor casing line on a two-stage transonic axial fan. The appropriate solution was selected from the Pareto front obtained by optimization as the final optimization structure. The calculation results were compared and analyzed. The results showed that the optimization structure achieved the optimization objective of expanding the stability margin of the compressor while not reducing or even increasing the peak efficiency at the design speed. Zuo [13] conducted multi-objective optimization research for the suction groove casing treatment on a centrifugal compressor. The objective functions were the isentropic efficiency at the design point and near the stall point. The constraints were the choked flow rate and the total pressure ratio at the design point and near the stall point. The multi-objective optimization and analysis of the geometric structure of the casing treatment were carried out, and the optimal Pareto front solution set was obtained. After adopting the best casing treatment with comprehensive performance, the compressor's comprehensive stability margin and isentropic efficiency at the design point and near stall point were significantly improved. Wang [14] conducted multi-objective optimization research for the groove casing treatment on a high-pressure compressor. The casing treatment structure that can simultaneously improve the efficiency and stability margin of the compressor was obtained, and the performance and flow field were analyzed in detail. Ba et al. [15,16] built a multi-objective optimization platform based on B-spline curve modeling for axial slots on a high-load, mixed-flow compressor. Three typical axial slot designs were selected from the optimization results, and the stability margin and efficiency indicators were comprehensively considered. The final axial slot

casing treatment obtained a 19.84% improvement in stability margin with only a loss of 0.28% peak efficiency.

Multi-objective optimization is a very effective method for optimizing the design of casing treatment. Compared with the traditional trial-and-error/iterative design, this method can clearly obtain the casing treatment structure that meets the optimization objectives, reducing blindness. For the casing treatment structure that seeks to balance the efficiency and stability margin of the compressor, it is a good solution. Therefore, in the current study, a numerical optimization study of a single groove was conducted on a high-speed axial compressor. The main aims of the study were (1) to find the optimal structure of a single groove casing treatment that can improve compressor stability with minimal loss in efficiency, (2) to reveal the influence of the circumferential groove design parameters on the stall margin and efficiency of the compressor, and (3) to explore suitable parameters for rapidly evaluating the compressor stall margin.

## 2. Study Model and Optimization Method

### *2.1. Investigated Compressor Model*

This study was conducted on a high-speed subsonic axial compressor test rig. The compressor rotor was equipped with 30 blades featuring Russia K70 series profile sections, and the design parameters of the compressor rotor are detailed in Table 1. The compressor test rig is illustrated in Figure 1. The investigations were all conducted at 70% of the design rotational speed for the compressor rotor.

**Table 1.** The design parameters of the compressor rotor.

| Parameter | Value |
|---|---|
| Design rotating speed (rpm) | 15,200 |
| Design mass flow rate (kg/s) | 5.6 |
| Design total pressure ratio | 1.249 |
| Design isentropic efficiency | 0.905 |
| Number of blades | 30 |
| Casing diameter (mm) | 298 |
| Tip clearance (mm) | 0.3 |
| Hub-tip ratio | 0.61 |

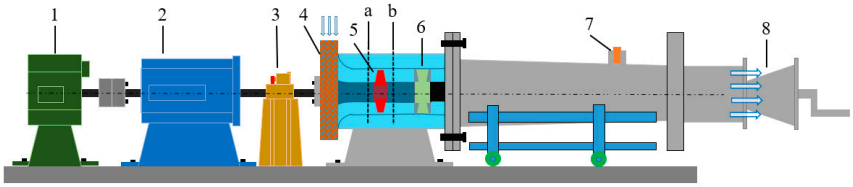



**Figure 1.** The compressor test rig. 1: DC motor; 2: Accelerator; 3: Torque meter; 4: Intake steel cover; 5: Rotor disk; 6: Stator disk; 7: Orifice flowmeter; 8: Throttle valve. a: Rotor inlet probe location; b: Rotor outlet probe location.

### *2.2. Parameterization of Groove Geometry*

The single circumferential groove is parameterized, as shown in Figure 2. The parameters include groove position, groove depth, groove width, and groove inclination angle. To explore a wider range of single circumferential groove structures, the geometric parameters are given with relatively large variation ranges. As shown in Table 2, the groove position can vary from 0 to 1.0 $C_{ax}$, the groove depth can vary from 0.01 to 1.0 $C_{ax}$, the groove width can vary from 0.01 to 1.0 $C_{ax}$, and the groove inclination angle can vary from −75 to 75 degrees. When the groove is inclined to the blade leading edge, the inclination angle is defined as negative; when the groove is inclined to the blade trailing edge, the inclination angle is defined as positive.

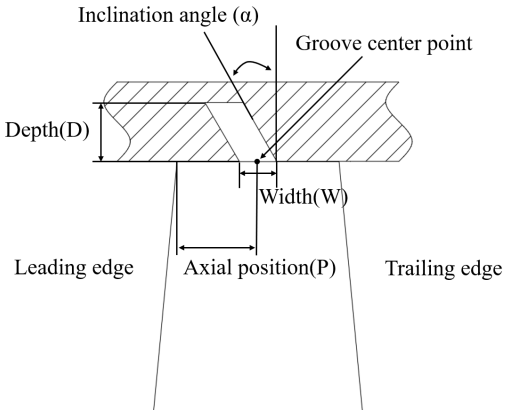



**Figure 2.** The structure of circumferential groove casing treatment.

**Table 2.** The design parameters and value ranges.

| Parameter | Symbol | Min | Max |
|---|---|---|---|
| Groove position | P | 0 $C_{ax}$ | 1.0 $C_{ax}$ |
| Groove depth | D | 0.01 $C_{ax}$ | 1.0 $C_{ax}$ |
| Groove width | W | 0.01 $C_{ax}$ | 1.0 $C_{ax}$ |
| Groove inclination angle | α | −75° | 75° |

### *2.3. Numerical Method and Validation*

This numerical investigation employed NUMECA, a computational fluid dynamics (CFD) software. The full three-dimensional Reynolds-Averaged Navier–Stokes equations were solved by using the Spalart–Allmaras turbulence model. Inlet boundary conditions employed airflow direction, total pressure, and total temperature, while the outlet boundary condition employed average static pressure. No-slip and no-heat transfer conditions were applied to all solid surfaces. Convergence of the calculation was achieved based on the following:

(a) Residuals root mean square: $< 1 \times 10^{-5}$.
(b) Mass flow rate: –Fluctuation (last 500 steps): < 0.001 kg/s. –Relative error (inlet vs. outlet, last 500 steps): < 0.2%.
(c) Total pressure and efficiency variation (last 500 steps): <0.2%.

Figure 3 illustrates the single-passage numerical model of the rotor with a single-groove casing treatment. Structured grids were used: "H" mesh in the inlet, outlet extensions, and grooves, "O" mesh around the rotor blades, and "butterfly" mesh in the rotor tip clearance. The total grid number reached approximately 1.5 million. The y+ is maintained at less than 3. The model was divided into two parts: a stationary inlet and a rotating section (rotor passage, outlet, and groove casing treatment).

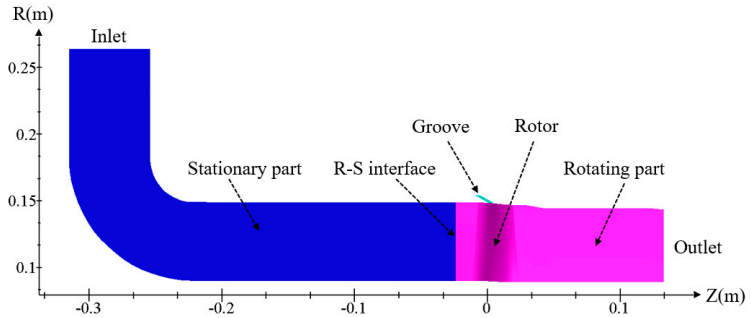



**Figure 3.** The numerical simulation model.

Due to the significant geometric variations of the single circumferential groove, in order to ensure the reliability of the single groove calculations in numerical simulations, a grid independence verification was conducted based on the maximum limit structure of the single circumferential groove. As shown in Figure 4, the total pressure ratio and efficiency of the compressor remain almost unchanged after the groove grid configuration of the single groove is increased to Mesh 4. Therefore, considering both calculation accuracy and time consumption, the groove grid configuration of Mesh 5 was selected in the present study. In addition, the numerical method used in this study has been shown in previous studies [17] to be able to accurately simulate the stability and performance trends of compressors with different groove casing treatments. Figure 5 shows the comparison of experimental and calculated results between the solid casing and three kinds of groove casing treatments. These three kinds of groove casing treatments have four grooves that cover the whole tip chord, and each groove has a 4.25 mm axial width and 6mm depth. The only difference is that Grooves 1 to 3 are inclined with −30, 0, and 30 degrees, respectively. As shown in Figure 5, there are some differences between the calculated and experimental values of the groove casing treatments. The calculated near-stall mass flow ratio of different groove casing treatments is smaller than the experimental value. This may be due to the difference between the compressor numerical model and the actual compressor, such as the tip clearance size varying around the circumference of the actual compressor and measurement errors in the experiment. But, the trend of the near-stall mass flow ratio of different groove casing treatments in numerical results is basically consistent with the experimental results. Although there are some differences in the values, the present numerical simulations are reliable for the present study to reveal the relevant laws and flow mechanisms.

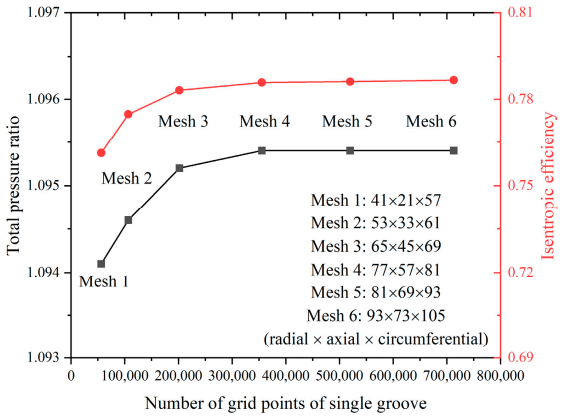



**Figure 4.** Grid independence verification of groove.

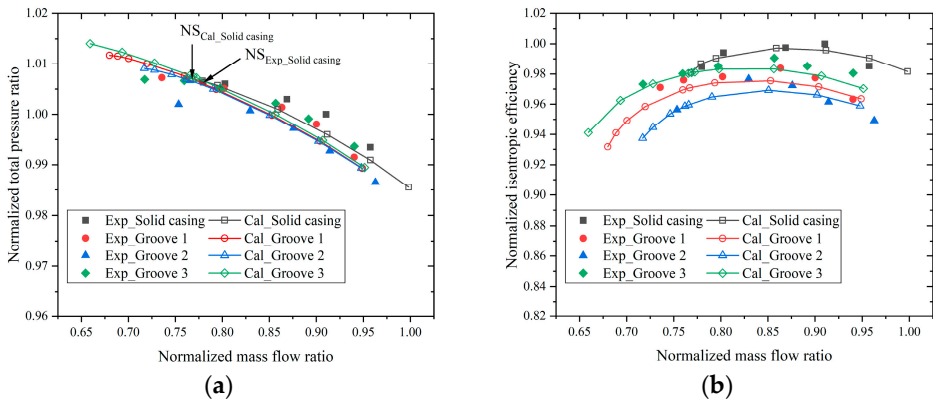



**Figure 5.** Experimental and calculated results for the overall performance of the rotor. (**a**) Normalized total pressure ratio; (**b**) normalized isentropic efficiency.

### *2.4. Optimization Method*

To obtain the single circumferential groove structure that balances compressor stability and efficiency, this paper adopts a multi-objective optimization method. In multi-objective optimization, the stall margin improvement (SMI) and peak efficiency improvement (PEI) are used as objective functions.

$$\max f_1 = SMI = \left( \frac{\pi^*_{ct,ns}}{\pi^*_{sc,ns}} \cdot \frac{M_{sc,ns}}{M_{ct,ns}} - 1 \right) \times 100\% \quad (1)$$

$$\max f_2 = PEI = \frac{\eta^*_{ct,peak} - \eta^*_{sc,peak}}{\eta^*_{sc,peak}} \times 100\% \quad (2)$$

where $\pi^*$ represents the total pressure ratio, $M$ denotes the corrected mass flow rate, and $\eta^*$ represents the isentropic efficiency. The $ct$, $sc$, $ns$, and $peak$ subscripts represent casing treatment, solid casing, near-stall point, and peak efficiency point, respectively.

Figure 6 shows the circumferential groove multi-objective optimization process. First, the single circumferential groove is parameterized, as described in Section 2.2. Then, 50 initial data samples are sampled using the optimal Latin hypercube method. In theory, the initial optimization database must be at least five times the size of the optimization variables. After numerical calculation, 36 initial optimization databases are formed by removing bad points. In the multi-objective optimization process, a Radial Basis Function (RBF) neural net surrogate model and NSGA-II multi-objective optimization algorithm are used to update the database. To obtain the real objective function values of the Pareto solutions, an in-house auto CFD solution code is applied in the CFD solution process. Finally, the convergent Pareto optimal solution is obtained after 30 iterations, and about 300 groove casing treatment individuals are evaluated. For each groove casing treatment individual, the compressor stall margin can be determined by calculating at least 8 numerical simulations under different outlet static pressure conditions.

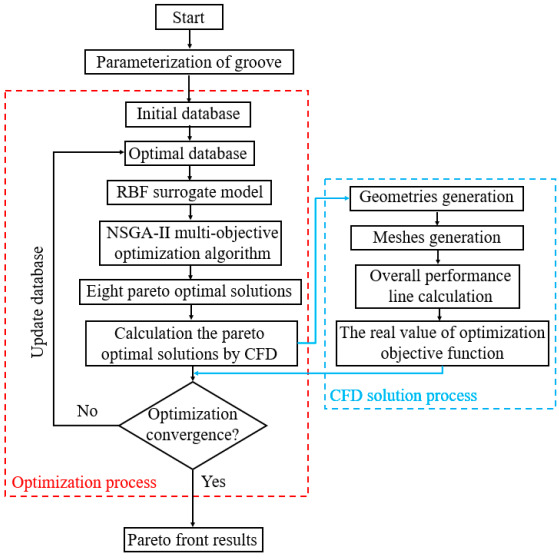



**Figure 6.** The circumferential groove multi-objective optimization process.

## 3. Results and Discussion

### *3.1. Optimization Results*

The optimization process evaluated a database of approximately 300 groove casing treatment individuals. And the optimization process reached convergence at the Pareto front. As shown in Figure 7, the red dashed line represents the Pareto front, and the green pentagon represents the original solid casing case. After the optimization process, the Pareto solutions eventually cluster around the Pareto front. Three typical Pareto front

solutions, A, B, and C, were selected from the Pareto front, as shown in the three red bullets of Figure 7. Figure 8 shows the overall performance curve of these three typical groove structures. And Table 3 shows the design parameters and corresponding objective function values for these three typical structures. The Case A solution has the highest objective function value for SMI, while the Case C solution has the highest objective function value for PEI. The Case B design achieved an SMI of 7.49% and a PEI of 0.24%, which can balance the stall margin and efficiency of the compressor. This makes it a more attractive option than the other designs, which either have a lower stall margin or a lower efficiency.

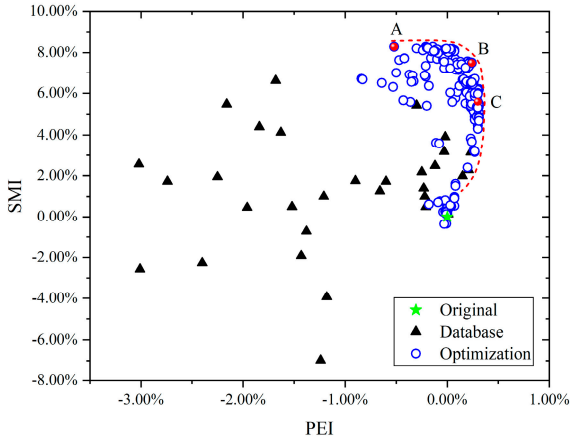
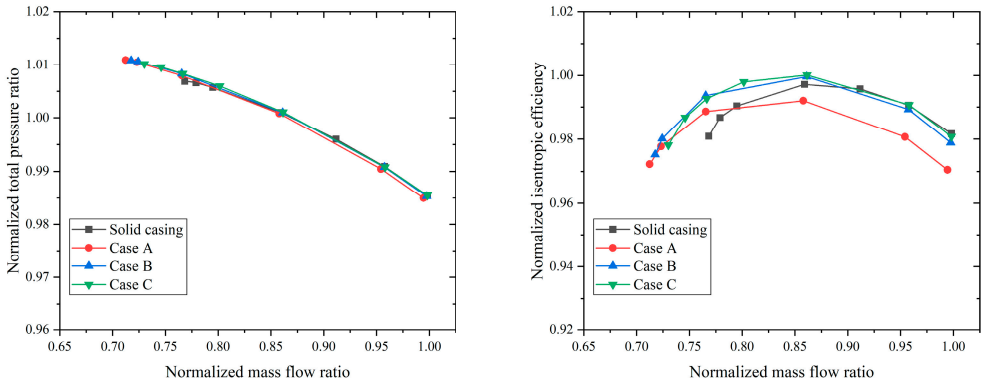



**Figure 7.** Optimization database.




(**a**) (**b**)

**Figure 8.** The overall performance of three typical groove structures. (**a**) Normalized total pressure ratio; (**b**) normalized isentropic efficiency.

**Table 3.** The typical groove parameters and objective functions.

| Case | $P/C_{ax}$ | $D/C_{ax}$ | $W/C_{ax}$ | $\alpha/^{\circ}$ | SMI | PEI |
|---|---|---|---|---|---|---|
| A | 0.366 | 0.997 | 0.323 | −56.4 | 8.28% | −0.52% |
| B | 0.394 | 0.321 | 0.198 | −60.9 | 7.49% | 0.24% |
| C | 0.473 | 0.762 | 0.157 | −64.3 | 5.59% | 0.30% |

### *3.2. Analysis of Design Parameters*

To reveal the influence of the circumferential groove design parameters and their interactions on SMI and PEI (objective functions), a design parameter sensitivity analysis based on the Sobol index method was conducted for the circumferential groove design parameters. The importance ranking of the design parameters was given according to the magnitude of the influence.

The Sobol index method is a global sensitivity analysis method that uses variance decomposition to define sensitivity indices. It has the advantages of being easy to understand, easy to calculate, and applicable to nonlinear or non-monotone models. This section provides a brief introduction to the sensitivity definition in the Sobol index method [18]. Suppose the relationship between the input variable $X = [X_1, X_2, \ldots, X_m]$ and the output variable $Y$ of a model is $Y = f(X)$. According to the high-dimensional model description of the model response function, $f(X)$, can be expanded into $2^n$ function terms:

$$Y = f_0 + \sum_{i=1}^{m} f_i(X_i) + \sum_{1 \le i < j \le m}^{C_m^2} f_{ij}(X_i, X_j) + \cdots + f_{12\ldots m}(X_1, X_2, \ldots, X_m) \tag{3}$$

When the variables are independent, the variances of the left and right sides of Equation (3) can be obtained as follows:

$$D = \sum_{i=1}^{m} D_i + \sum_{1 \le i < j \le m} D_{ij} + \cdots + D_{1,2,\ldots,m} \tag{4}$$

It can be seen that Equation (4) decomposes the output variance of the model into $2^n - 1$ terms of increasing order, which can be used to describe the variances caused by each input variable and its interactions. Therefore, the contribution of each input variable to the variance of the output variable can be measured by the ratio of the variance of each term to the total variance of the output variable. This leads to the definition of sensitivity indices:

$$S_{i_1,\ldots,i_s} = \frac{D_{i_1,\ldots,i_s}}{D} (1 \le i_1 < \ldots < i_s \le m) \tag{5}$$

Substituting Equation (4), we get the following expression:

$$\sum_{i=1}^{m} S_i + \sum_{1 \le i < j \le m} S_{ij} + \cdots + S_{1,2,\ldots,m} = 1 \tag{6}$$

The first-order index $S_i$ is the main effect index, and its definition is given in Equation (7). It represents the individual contribution of each input variable to the variance of the output variable. The second-order sensitivity index, $S_{ij}$, is defined as Equation (8), which can measure the contribution of the interaction between two input variables to the output variance.

$$S_i = \frac{D_i}{D} (i = 1, \ldots, m) \tag{7}$$

$$S_{ij} = \frac{D_{ij}}{D} (1 \le i < j \le m) \tag{8}$$

The total effect index of $X_i$ is defined as the sum of all sensitivity indices on the left side of Equation (6) that include the index $i$:

$$S_i^T = \sum_{\Omega_i} S_{i_1,\ldots,i_s}, \Omega = \{(i_1, \ldots, i_s) : \exists k, 1 \le k \le s, i_k = i\} \tag{9}$$

The total effect index, $S_i^T$, can measure the total contribution of the input variable $X_i$ itself and its interactions with other variables of all orders to the variance. According to Equation (6), the total effect index, $S_i^T$, can also be indirectly calculated by the first-order partial variance of the input vector, $X_{\sim i}$, containing all input variables except $X_i$:

$$S_i^T = 1 - \frac{D_{\sim i}}{D} \tag{10}$$

In this section, the design parameters of the circumferential groove are selected as input variables, and the optimization objective function is selected as the output variable to establish a global sensitivity analysis model. About 10,000 sample points were sampled based on the Sobol sequence method. In order to save computing time and resources, this paper directly uses the RBF neural network surrogate model trained during the optimization process to estimate the model output values required in the sensitivity calculation process. That is, the RBF neural network surrogate model is used as the object of sensitivity analysis.

Figure 9 shows the results of the sensitivity analysis of the design parameters for objective function SMI. As shown in Figure 9a, the design parameter importance ranking obtained according to the size of the main effect index is $W > \alpha > P > D$. The importance ranking obtained according to the size of the total effect index is also $W > \alpha > P > D$. It can be seen that parameters $W$ and $\alpha$ have a significant impact on the stall margin of the compressor, while the impact of parameters $P$ and $D$ is small. In addition, it can be noted that the main effect index and total effect index of parameters $P$ and $W$ are significantly different, indicating that their interaction with other parameters also has a significant impact on the stall margin. As shown in the second-order sensitivity index heat map in Figure 9b, the interaction between $P$ and $W$ has the most significant impact on the stall margin.

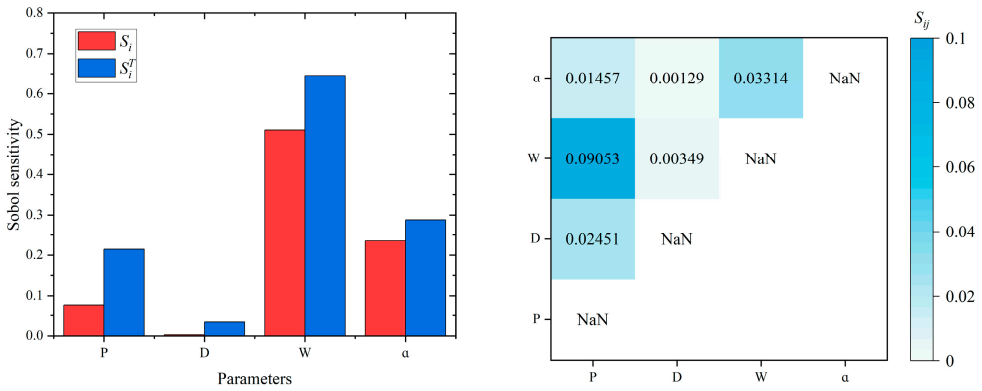
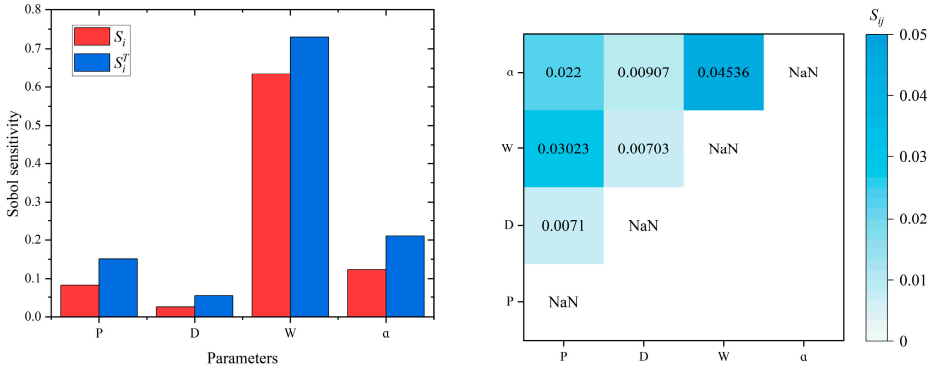



**Figure 9.** Sensitivity index of design parameters to stall margin improvement. (**a**) Main effect index and total effect index; (**b**) second-order sensitivity index.

Figure 10 shows the results of the sensitivity analysis of the design parameters for objective function PEI. As shown in Figure 10a, the design parameter importance ranking obtained according to the size of the main effect index is $W > \alpha > P > D$. The importance ranking obtained according to the size of the total effect index is also $W > \alpha > P > D$. It can be seen that parameter $W$ has a significant impact on the peak efficiency of the compressor, while the impact of parameters $P$, $D$, and $\alpha$ is small. In addition, it can be noted that the main effect index and total effect index of parameters $P$, $W$, and $\alpha$ are significantly different, indicating that their interaction with other parameters also has a significant impact on the peak efficiency. As shown in the second-order sensitivity heat map in Figure 10b, the interaction between $\alpha$ and $W$ has the most significant impact on the peak efficiency.

The above research found that stall margin, groove width ($W$), groove inclination angle ($\alpha$), and the interaction between groove position ($P$) and groove width ($W$) have a significant impact on the SMI. For efficiency, groove width ($W$) and the interaction between groove width ($W$) and groove inclination angle ($\alpha$) have a significant impact on the PEI. When designing a single circumferential groove, these parameters should be given priority.




(**a**) (**b**)

**Figure 10.** Sensitivity index of design parameters to peak efficiency improvement. (**a**) Main effect index and total effect index; (**b**) second-order sensitivity index.

The above sensitivity analysis can only obtain the importance of the impact of design parameters on the objective function, but it cannot reveal the law of change of the objective function with the design parameters. In order to further analyze the law of change of the objective function with different design parameters, the scatter distribution of Pareto optimal solutions under the objective function SMI and PEI are first given in Figures 11 and 12. The red bullets denote Pareto optimal solutions and the blue bullets denote all database solutions. As shown in Figures 11 and 12, the red hollow circles represent the Pareto front optimal solutions, and the blue hollow circles represent all the sample points during the optimization process. Under the optimal stall margin objective function, the single circumferential groove geometry presents the following features: the groove position is close to the tip leading edge (about 0.2–0.5 $C_{ax}$), the groove is narrow (about 0.2–0.4 $C_{ax}$), the groove is inclined upstream by about −60 degrees, and the groove depth has little effect on the stall margin. Under the optimal peak efficiency objective function, the single circumferential groove geometry presents the following features: the groove position is close to about 0.4 $C_{ax}$, the groove is narrow (about 0.2 $C_{ax}$), the groove is also inclined upstream by about −60 degrees, and the groove depth also has little effect on the peak efficiency.

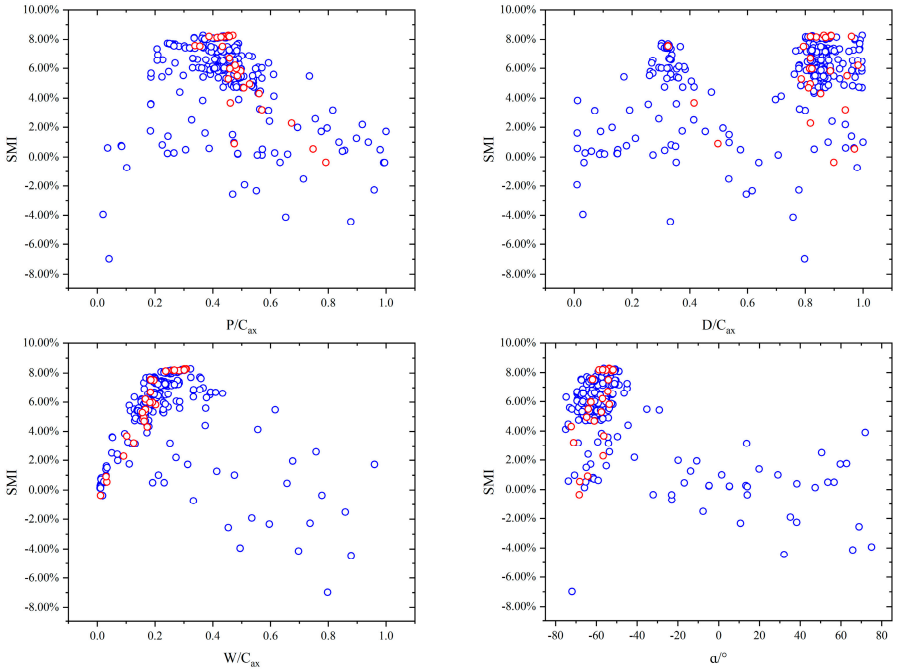



**Figure 11.** Optimal circumferential groove geometric parameter distribution under SMI objective function.

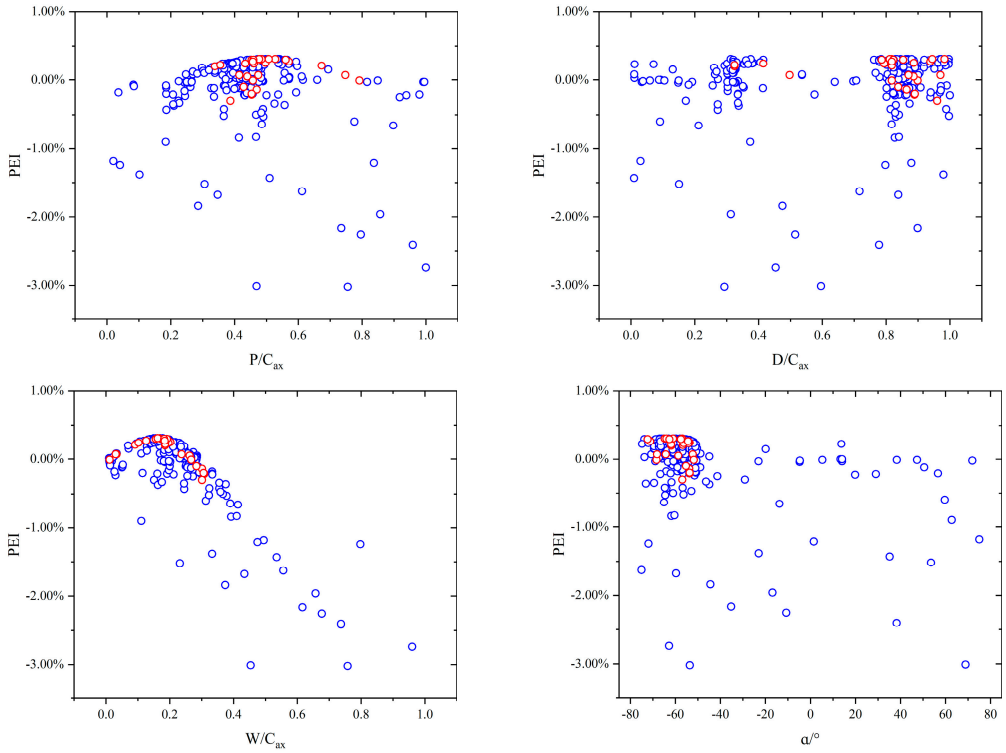



**Figure 12.** Optimal circumferential groove geometric parameter distribution under PEI objective function.

Figure 13 further shows the change curves of the predicted values of the objective function by the surrogate model when other parameters are given according to the optimal solution Case B. As shown in Figure 13 for the groove position, its impact on SMI and PEI is not monotonic. The best stall margin improvement can be obtained when the groove position is between 0.2 and 0.4 $C_{ax}$, while the groove position has little impact on the peak efficiency. However, the best peak efficiency improvement can be obtained when the groove position is about 0.4 $C_{ax}$. For the groove depth, its impact on SMI and PEI is very small, and both shallow and deep grooves can obtain the best objective function value. For the groove width, its impact on SMI and PEI is relatively large. The best stall margin improvement can be obtained when the groove width is about 0.2 $C_{ax}$, while a smaller groove width can obtain a larger peak efficiency improvement. For the groove inclination angle, the best stall margin improvement can be obtained when the groove is inclined upstream by about 60 degrees. Additionally, a larger upstream inclination angle can lead to a larger peak efficiency improvement.

RBF neural network surrogate models are trained on a large number of samples to obtain the prediction ability of the model output. However, the predicted laws are difficult to guarantee to be completely consistent with the actual situation due to the lack of constraints on the physical mechanism and strong dependence on samples. However, based on the previous parameter analysis, the basic laws of the influence of single circumferential groove design parameters on SMI and PEI can be summarized as follows: the groove position close to the tip leading edge (0.2–0.5 $C_{ax}$) can obtain a larger stall margin improvement, and the groove position is near about 0.4 $C_{ax}$ can obtain the best peak efficiency improvement. The groove depth has little influence on the stall margin and peak efficiency. The groove width has a greater influence on the stall margin and peak efficiency. A narrow groove (about 0.2–0.4 $C_{ax}$) can obtain the best stall margin improvement and peak efficiency improvement. When the groove is inclined upstream by a certain angle (about 60 degrees), the best stall margin improvement and peak efficiency improvement can be obtained.

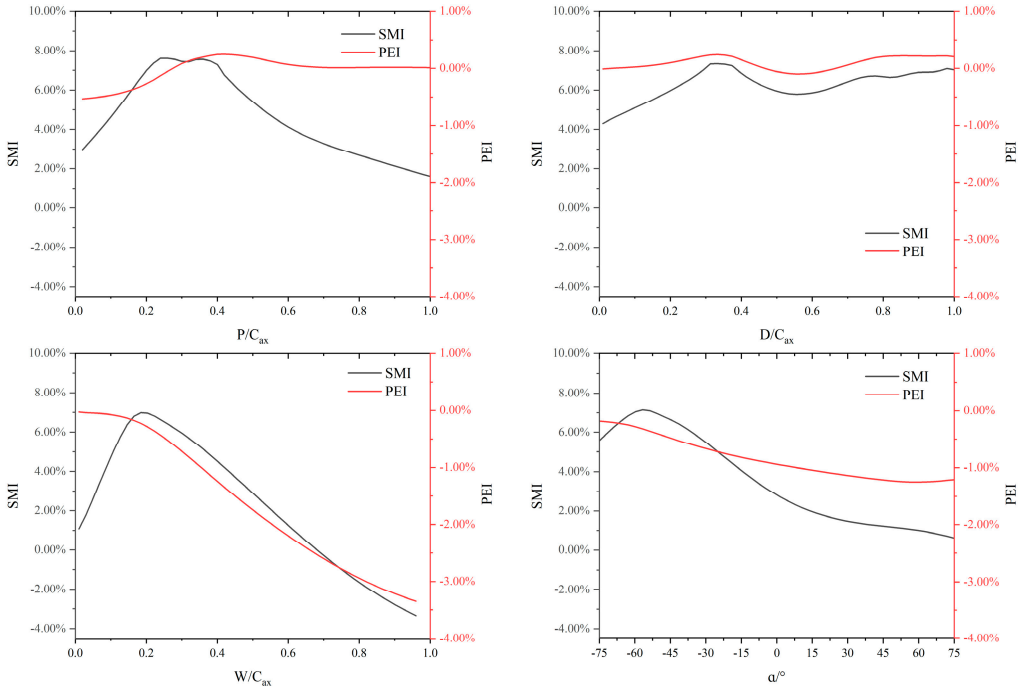


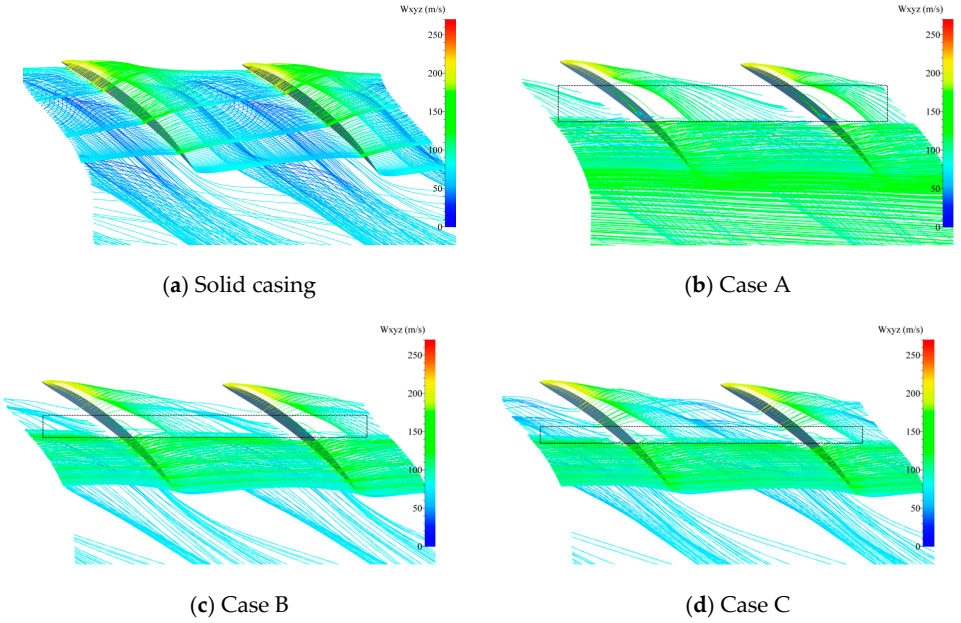

**Figure 13.** The law of change of the predicted value of the objective function with the design parameters.

### *3.3. Analysis of Flow Mechanism*

To further elucidate the inherent flow mechanism of the circumferential single-groove structures on the Pareto front, a flow mechanism analysis was conducted for three typical circumferential single-groove structures. Based on our previous research experience, the application of circumferential groove casing treatment significantly alters the flow structure in the blade tip region of compressors, particularly the flow structure of the blade tip leakage flow.

Figure 14 shows the distribution of tip leakage flow under the same near-stall condition of solid casing, with solid casing and three groove structures. And the tip leakage flow lines are rendered by the value of relative velocity. It can be seen from Figure 14a that under the near-stall condition of the solid casing, the tip leakage flow fills the entire blade tip passage. The tip leakage flow is expanded and dispersed, and it is almost parallel to the line connecting the blade tip's leading edge. This seriously hinders the flow of air at the blade tip passage. However, when a circumferential single groove is applied, the tip leakage flow becomes significantly more concentrated, and the tip leakage flow is significantly shifted towards the blade suction surface. The tip leakage flow is significantly removed, so the degree of blockage of the blade tip passage is significantly reduced. Figure 14 clearly shows that the Case A solution exhibits the greatest reduction and concentration of blade tip leakage flow streamlines. This indicates that the Case A solution has the strongest suppressive effect on the leakage flow, leading to the largest improvement in stall margin. Figure 15 further illustrates the entropy distribution of 99% span at the same near-stall condition of solid casing. The interface between the tip leakage flow and the mainstream can be easily distinguished from the interface between high entropy value and low entropy value. When the solid casing is at near-stall condition, the interface between the tip leakage flow and the mainstream is almost flush with the line connecting the blade tip leading edge. This significantly hinders the flow of mainstream, ultimately leading to the stall of the compressor. However, when a circumferential single groove is applied, it can be clearly observed that the interface between the tip leakage flow and the mainstream is shifted towards the suction surface of the adjacent blade. And the shift of the Case A solution is slightly larger than that of the other two circumferential single-groove structures. Therefore, the Case A solution has the best improvement effect on the blade tip passage of

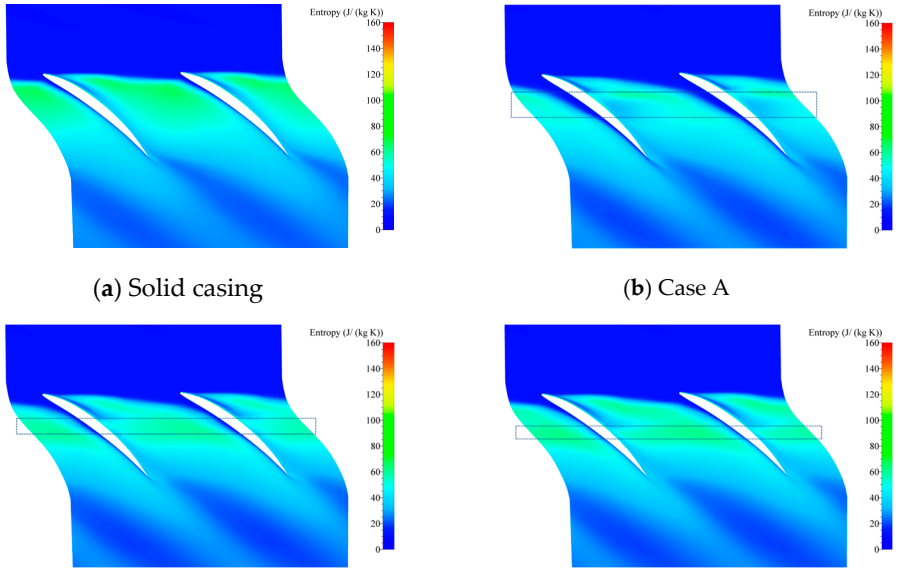
the compressor and thus obtains the largest stability margin improvement among these three groove structures.




(**a**) Solid casing (**b**) Case A

(**c**) Case B (**d**) Case C

**Figure 14.** The tip leakage flow distribution at near-stall condition of solid casing.



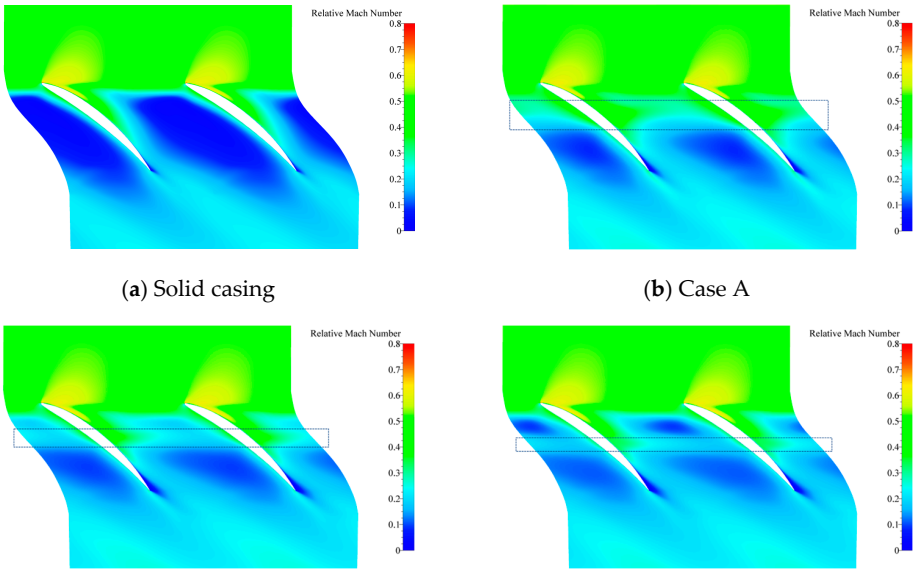

(**a**) Solid casing (**b**) Case A

(**c**) Case B (**d**) Case C

**Figure 15.** The entropy distribution at near-stall condition of solid casing.

Figure 16 further shows the relative Mach number distribution cloud map at 99% span under the same near-stall conditions of solid casing. It can be seen from the solid casing that under near-stall conditions, the compressor tip passage is filled with a large number of blue low-relative Mach number regions. It almost occupies the entire blade tip passage, so the blade tip flow condition has significantly deteriorated. However, with the application of the circumferential single groove, the low-speed region at the blade tip passage is significantly reduced, particularly within the blade leading edge passage where the relative Mach number was previously very low. Figure 16 clearly reveals significant variations in the effectiveness of different single-groove designs on the blade tip flow field. The Case A

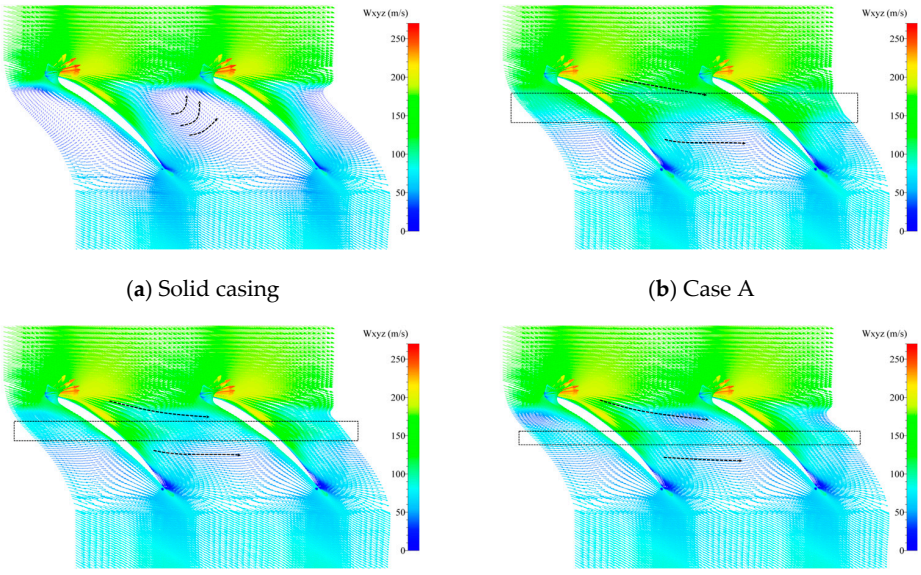
solution demonstrates the most significant improvement, particularly at the leading edge, followed by the Case B solution. The Case C solution exhibits the least improvement. The impact of all three groove designs on the blade trailing edge flow field shows generally moderate improvement. Figure 17 further shows relative velocity vector distribution at 99% span under the same near-stall condition of solid casing. Figure 17 shows that under near-stall conditions with a solid casing, the compressor blade tip passage suffers from significant backflow. This backflow severely restricts the blade tip passage, leading to a deterioration of the flow field in that region. Consequently, compressor instability is further induced. However, after the circumferential groove is applied, the blade tip backflow is significantly eliminated. Compared with the other two single groove structures, the airflow direction near the blade tip leading edge of the Case A structure is more inclined towards the suction surface of the adjacent blade, and the airflow flow conditions are better.




(**a**) Solid casing (**b**) Case A

(**c**) Case B (**d**) Case C

**Figure 16.** The relative Mach number distribution at near-stall condition of solid casing.




(**a**) Solid casing (**b**) Case A

(**c**) Case B (**d**) Case C

**Figure 17.** The relative velocity vector distribution at near-stall condition of solid casing.

The above qualitative analysis from the flow field perspective has revealed the mechanism that influence different circumferential groove geometries on the blade tip flow of the compressor. In the following, a quantitative analysis is conducted to compare the influence of different circumferential groove geometries on the stability of the compressor.

In our previous study [17], we found that tip blockage can be used to effectively evaluate the trend of the stall margin. The tip blockage was defined as the decrease in effective flow area and was expressed as shown in Equation (11):

$$B = 1 - \frac{A_{eff}}{A} = 1 - \frac{A - \int \delta^* dr}{A} \tag{11}$$

where $B$ represents tip blockage, $A$ represents the geometrical section area of blade passage along axial direction, $A_{eff}$ represents the effective core flow area of blade passage along axial direction under the effect of tip blockage, r represents the radial direction, and $\delta^*$ represents the integral of the density–velocity deficit across the blade passage. The $\delta^*$ represents a function of radius and is expressed as shown in Equation (12):

$$\delta^*(r) = \int_0^{\frac{2\pi}{NB}} \left(1 - \frac{\rho w_z}{\overline{\rho w_z}}\right) r d\theta \tag{12}$$

where $NB$ represents the number of rotor blade, $\theta$ denotes the circumferential direction, $\rho$ represents density, $w_z$ represents relative axial velocity, and $\overline{\rho w_z}$ represents the average $\rho w_z$ of the calculation section along the axial direction. The density–velocity deficit region was determined by the sum of radial and circumferential gradients of $\rho w_z$ with respect to a suitable cutoff value and is expressed as shown below:

$$\left|\frac{\partial(\rho w_z)}{\partial r}\right| + \left|\frac{\partial(\rho w_z)}{\partial(r\theta)}\right| \geq cutoff \tag{13}$$

As can be seen from Figure 18, when a circumferential groove casing is applied, the degree of blockage in the blade tip passage is significantly reduced compared to the solid casing, and the flow conditions in the blade tip passage are significantly improved. The three single-groove structures exhibit significant variations in their effectiveness at reducing blockage near the blade tip leading edge. Notably, Case A demonstrates the greatest improvement in this critical region, which aligns with its observed increase in stability margin. The quantitative analysis of blade tip blockage shows that there is a certain correlation between the degree of blade tip blockage under the action of circumferential grooves and the stability margin of the compressor.

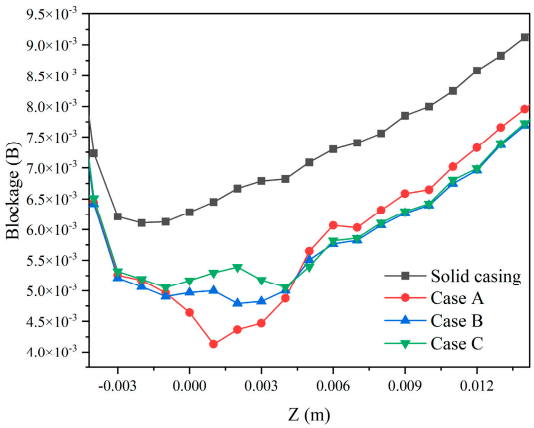



**Figure 18.** The tip blockage distribution along axial direction at near-stall condition of solid casing.

The airflow at the compressor tip enters and exits the groove, producing a momentum transport effect on the tip flow field. Two parameters, circumferential mass flow flux in the

groove ($M_t$) and radial transport momentum of the circumferential transport flux ($Mo_r$), are introduced to evaluate the impact of the momentum transport effect caused by the groove.

$$M_t = \iint \rho w_t dA_1 \tag{14}$$

$$Mo_r = \iint \rho w_t w_r dA_2 \tag{15}$$

where $A_1$ represents the groove section area in the circumferential direction, $A_2$ represents the groove bottom area (as shown in Figure 19), $w_t$ represents the circumferential component of relative velocity, and $w_r$ represents the radial component of relative velocity.

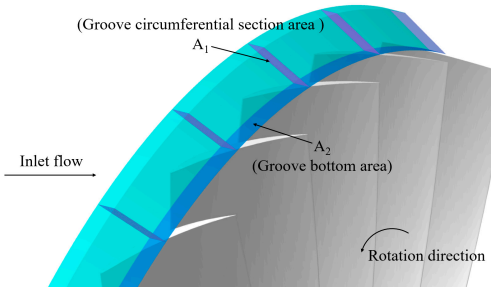



**Figure 19.** A schematic diagram of the $A_1$ and $A_2$ for calculation of momentum transport effect.

Figure 20 shows the momentum transport effect of the circumferential single groove on the blade tip flow field. It can be seen that the trend of the circumferential mass flow flux and the stability expansion ability of the circumferential single groove is not consistent. In contrast, the radial transport momentum of the circumferential single groove exhibits a strong correlation with its stability expansion ability. A higher radial transport momentum value corresponds to a greater radial transport effect on the blade tip passage and, consequently, a stronger stability expansion ability of the circumferential single groove.

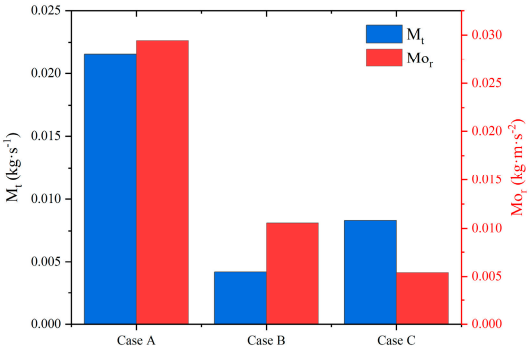



**Figure 20.** The momentum transport effect of three groove structures at near-stall condition of solid casing.

The application of a single groove changes the momentum balance state at the tip of the compressor. To quantitatively evaluate this momentum balance state, the momentum ratio ($MR$) parameter is introduced [19].

$$MR = \frac{Mo_{Tp}}{Mo_{Ic}} \tag{16}$$

where $Mo$ represents the momentum. The $I$, $T$, $c$, and $p$ subscripts represent the inlet flow, tip leakage flow, chordwise direction, and perpendicular to chordwise direction, respectively. A schematic diagram of the surface for the calculation of the momentum ratio is shown in Figure 21.

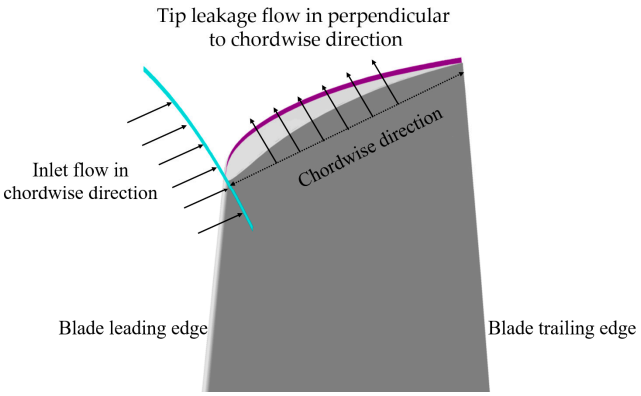



**Figure 21.** A schematic diagram of the surface for calculation of momentum ratio.

Figure 22 shows that after the application of the circumferential single groove, the momentum ratio is significantly reduced. The dynamic balance state of the blade tip flow field is changed, the dominant role of the tip leakage flow is significantly reduced, and the blade tip flow condition is improved. Therefore, the smaller the momentum ratio, the stronger the stability expansion ability of the circumferential single groove, and the more obvious the correlation between it and the strength of the stability expansion ability of the circumferential single groove.

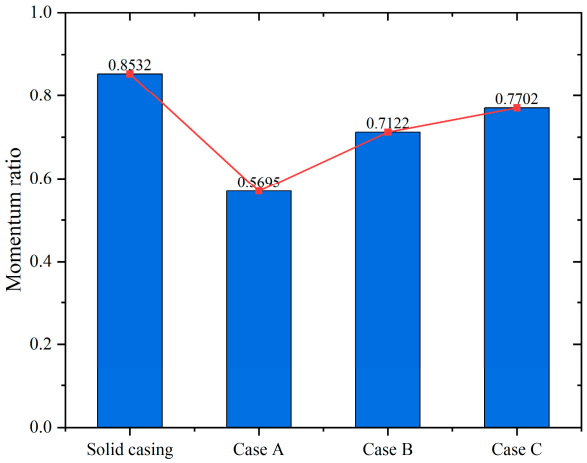



**Figure 22.** The momentum ratio of three groove structures at near-stall condition of solid casing.

To analyze the effect of different circumferential single grooves on compressor efficiency, Figure 23 shows the meridional entropy value integration of the solid casing and three circumferential single grooves at the same mass flow ratio. And this mass flow ratio is the same as the mass flow ratio under the peak-efficiency condition of the solid casing. It can be seen that when the Case A solution is applied, the integral entropy value is significantly increased compared to the solid casing, indicating that the loss of the compressor is significantly increased after applying the Case A solution, leading to a greater compressor efficiency loss. However, when the Case B solution and the Case C solution are applied, the integral entropy value is significantly reduced compared to the solid casing, indicating that the loss of the compressor is significantly reduced after applying the Case B and the Case C solutions, and the compressor efficiency loss is reduced.

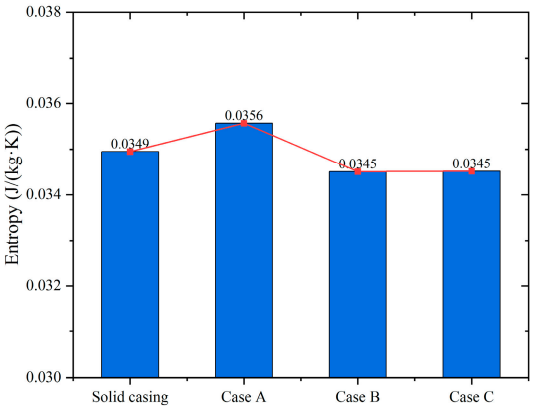



**Figure 23.** The integral entropy of meridian plane at peak-efficiency condition of solid casing.

### *3.4. Analysis of Stall Margin Evaluation Parameters*

In the optimization process of this paper, the stall margin of each sample point is evaluated by calculating the entire overall performance line. Calculating the entire overall performance line of a compressor can provide a relatively accurate estimate of the compressor stall margin. In engineering applications, the computational cost of evaluating the stall margin by calculating the entire overall performance line is unacceptable, as the optimization process requires the calculation of a large number of sample points. Therefore, this paper evaluates a series of parameters, and the aim is to find an evaluation parameter for the stall margin under the near-stall mass flow ratio of solid casing condition to replace the calculation of the entire overall performance line.

These evaluation parameters include total pressure ratio, tip blockage, groove transport effect, and momentum ratio under the same near-stall mass flow ratio of the solid casing. In reference [16], they found that SMI is linearly proportional to the total pressure ratio at the near-stall mass flow ratio of the solid casing condition. So, the total pressure ratio ($\pi^*$) at the near-stall mass flow ratio of the solid casing condition is firstly considered to evaluate the SMI. Based on the above flow mechanism analysis, it is evident that tip blockage, the transport effect of the groove, the momentum ratio, and the stability expansion ability of the circumferential single groove exhibit a degree of correlation. Consequently, these parameters were chosen to evaluate the compressor stability margin. This work simultaneously evaluates the tip blockage at different axial chord positions (0 $C_{ax}$, 0.2 $C_{ax}$, 0.4 $C_{ax}$, 0.5 $C_{ax}$, 0.6 $C_{ax}$, 0.8 $C_{ax}$, and 1.0 $C_{ax}$), respectively represented by $B_1$–$B_7$.

Spearman correlation analysis was used to explore the evaluation ability of various stall margin evaluation parameters for the stall margin of the compressor with different groove CTs. Based on the optimization database, Spearman correlation analysis was carried out. Figure 24 shows the heat map distribution of the Spearman correlation coefficient. For a database, Spearman correlation analysis can provide the correlation degree and direction between variables, and it is one of the most common statistical methods for measuring multivariate correlation. When two variables are perfectly monotonically related, the Spearman correlation coefficient is +1 or −1, with a positive value representing positive correlation and a negative value representing negative correlation. When the correlation between two variables is more significant, the absolute value of the Spearman correlation coefficient approaches 1. In general, it is believed that the correlation between variables is considered to be strong when the correlation coefficient is between 0.8 and 1.0.

Figure 24 shows that $B_1$ and MR (shown in the red dashed rectangle) are significantly correlated with SMI, with Spearman correlation coefficients of −0.8254 and −0.8754, respectively. B1 and MR both are negatively correlated with SMI. Based on these results, in the optimization of the single circumferential groove, it is possible to use the tip blockage at the tip leading edge or momentum ratio parameters to evaluate the stall margin of different single circumferential groove structures. For each individual groove-casing treatment, this only requires the calculation of one operating condition at the near-stall flow rate of the

solid casing, without the need to calculate the entire overall performance line (at least eight operating conditions), which greatly reduces the optimization calculation time. The results facilitate the application of optimization methods to engineering practice by reducing the computational cost of optimization.

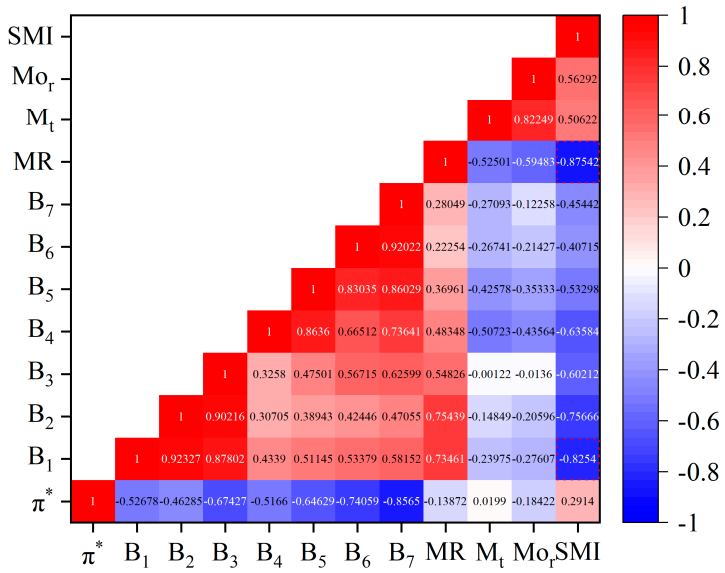



**Figure 24.** The stall margin evaluation parameter correlation analysis heat map.

## 4. Conclusions

In this paper, an optimization study of a single groove was conducted on a high-speed subsonic axial compressor. The optimal structure of a single groove casing treatment was obtained, which can improve compressor stability with improved compressor peak efficiency. This study revealed the regularity of the influence of single-groove design parameters on SMI and PEI. A relatively reliable and rapid stall margin evaluation parameter for the compressor has been obtained. Several conclusions are summarized as follows:

1. By the optimization study, one of the optimal single groove designs was found to achieve a 7.49% improvement in stall margin with a 0.24% improvement in peak efficiency.
2. For single-groove CTs, the groove width, inclination angle, and the interaction between groove position and groove width have a significant impact on the compressor stability. The groove width and the interaction between groove width and groove inclination angle have a significant impact on the compressor efficiency. The optimal groove presents the following geometric characteristics: the groove position is about 0.2–0.5 $C_{ax}$, the groove width is about 0.2–0.4 $C_{ax}$, and the groove inclination angle is near −60 degrees.
3. Among three typical Pareto front solutions, Case A, with the largest groove width, shows the strongest radial transport effect, and the tip blockage near the leading edge is the minimum. So, Case A shows the best stall margin improvement among these three Pareto front cases. The Case C solution, with the largest groove inclination angle upstream, shows the minimum entropy generation, and it also means the minimum flow loss. So, Case C shows the best peak efficiency improvement among these three Pareto front cases.
4. The stall margin evaluation parameters, B1 and MR, are significantly correlated with SMI, with Spearman correlation coefficients of −0.8254 and −0.8754, respectively. So, in the optimization of the single groove, the tip blockage at the tip leading edge or momentum ratio parameters can be calculated at the near-stall flow rate of the solid casing to evaluate the stall margin of the compressor with different single-groove structures. For each individual groove casing treatment, only one operating condition is needed to be calculated. This method can significantly reduce the optimization

time. And it also can be extended to the optimal design of passive casing treatment. Of course, we will further verify the reliability of this method in future studies.

**Author Contributions:** Conceptualization, W.C. and H.Z.; methodology, W.L.; software, W.L.; validation, W.L. and H.W.; formal analysis, W.L.; investigation, W.L.; resources, W.L.; data curation, W.L.; writing—original draft preparation, W.L.; writing—review and editing, W.L. and H.W.; visualization, W.L. All authors have read and agreed to the published version of the manuscript.

**Funding:** This research was funded by grant number 52076179 (National Natural Science Foundation of China) and grant number J2019-I-0011 (National Science and Technology Major Projects of China).

**Data Availability Statement:** The original contributions presented in the study are included in the article, further inquiries can be directed to the corresponding author.

**Conflicts of Interest:** The authors declare no conflicts of interest.

## References

1. Benser, W.A.; Finger, H.B. Compressor stall problems in gas-turbine-type aircraft engines. *SAE Trans.* **1957**, *65*, 187–200.
2. Greitzer, E.M. Surge and rotating stall in axial flow compressors-part I: Theoretical compression system model. *J. Eng. Power* **1976**, *98*, 190–198. [CrossRef]
3. Guo, Z.; Chu, W.; Zhang, H.; Liang, C.; Meng, D. Statistical evaluation of stability margin of a multi-stage compressor with geometric variability using adaptive polynomial chaos-Kriging model. *Phys. Fluids* **2023**, *35*, 076114. [CrossRef]
4. Koch, C. *Experimental Evaluation of Outer Case Blowing or Bleeding of a Single-Stage Axial-Flow Compressor*; Report: NASA-CR-54592, GE-R69AEG256; General Electric Co. (Aircraft Engine Group): Lynn, MA, USA, 1970; 86p.
5. Moore, R.D.; Kovich, G.; Blade, R.J. *Effect of Casing Treatment on Overall and Blade Element Performance of a Compressor Rotor*; Report: NASA-TN-D-6538, E-6119; National Aeronautics and Space Administration; Lewis Research Center: Cleveland, OH, USA, 1971; 65p.
6. Bailey, E.E. *Effect of Grooved Casing Treatment on the Flow Range Capability of a Single-Stage Axial-Flow Compressor*; Report: NASA-TM-X-2459, E-6560; National Aeronautics and Space Administration; Lewis Research Center: Cleveland, OH, USA, 1972; 15p.
7. Vuong, T.D.; Kim, K.Y.; Dinh, C.T. Recirculation-groove coupled casing treatment for a transonic axial compressor. *Aerosp. Sci. Technol.* **2021**, *111*, 106556. [CrossRef]
8. Goinis, G.; Voß, C.; Aulich, M. Automated optimization of an axial-slot type casing treatment for a transonic compressor. In *Turbo Expo: Power for Land, Sea, and Air*; American Society of Mechanical Engineers: San Antonio, Texas, USA, 2013; Volume V06BT43A011, p. 55232.
9. Goinis, G.; Nicke, E. Optimizing surge margin and efficiency of a transonic compressor. In *Turbo Expo: Power for Land, Sea, and Air*; American Society of Mechanical Engineers: Seoul, Republic of Korea, 2016; Volume V02AT37A048, p. 49699.
10. Kim, J.H.; Kim, D.W.; Kim, K.Y. Aerodynamic optimization of a transonic axial compressor with a casing groove combined with tip injection. *Proc. Inst. Mech. Eng. Part A J. Power Energy* **2013**, *227*, 869–884. [CrossRef]
11. Zhao, Q.J.; Zhou, X.Y.; Xiang, X.R. Multi-objective Optimization of Groove Casing Treatment in a Transonic Compressor. *Proc. Inst. Mech. Eng. Part A-J. Power Energy* **2014**, *228*, 626–637. [CrossRef]
12. Zhu, G. *Investigation of Stall Mechanism and Stabilization Enhancement Technology in a High Loaded Axial Compressor*; Northwestern Polytechnical University: Xi'an, China, 2017.
13. Zuo, P. *Stability Enhancement Mechanism and Multi-Optimization of Casing Treatment in a Transonic Centrifugal Compressor*; Tianjin University: Tianjin, China, 2018.
14. Wang, L. *Experiment Test and Optimization Design of Slope-Type Casing Treatment*; Shanghai Jiao Tong University: Shanghai, China, 2018.
15. Ba, D.; Du, J.; Zhang, Q.; Li, Z.; Zhang, H.; Nie, C.; Zhang, M. Design and optimization of casing treatment based on B-spline curves in a mixed-flow compressor. *J. Eng. Thermophys.* **2020**, *41*, 2171–2177.
16. Ba, D.; Zhang, Q.; Du, J.; Li, Z.; Zhang, H.; Nie, C. Design optimization of axial slot casing treatment in a highly-loaded mixed-flow compressor. *Aerosp. Sci. Technol.* **2020**, *107*, 106262. [CrossRef]
17. Liu, W.H.; Chu, W.L.; Zhang, H.G.; Zhang, C.Y. Effect of Inclination Grooves on Axial Flow Compressor Stability: An Experimental and Numerical Simulation Study. *J. Appl. Fluid Mech.* **2022**, *16*, 311–323. [CrossRef]
18. Saltelli, A.; Ratto, M.; Andres, T.; Campolongo, F.; Cariboni, J.; Gatelli, D.; Saisana, M.; Tarantola, S. Global sensitivity analysis. In *The Primer*; John Wiley & Sons: Chichester, UK, 2008; pp. 155–164.
19. Du, J.; Lin, F.; Zhang, H.; Chen, J. Numerical investigation on the self-induced unsteadiness in tip leakage flow for a transonic fan rotor. *J. Turbomach.* **2010**, *132*, 021017. [CrossRef]

**Disclaimer/Publisher's Note:** The statements, opinions and data contained in all publications are solely those of the individual author(s) and contributor(s) and not of MDPI and/or the editor(s). MDPI and/or the editor(s) disclaim responsibility for any injury to people or property resulting from any ideas, methods, instructions or products referred to in the content.